# Understanding the influence of fluid flow regime on plasma morphology and dose delivery at the plasma-liquid interface



R. Z. Walker Z ; J. E. Foster



Journal of Applied Physics 133, 093301 (2023) https://doi.org/10.1063/5.0141059





CrossMark

# Articles You May Be Interested In

Application of a bi-modal PBR nuclear propulsion and power system to military missions

AIP Conference Proceedings (January 1995)

Microwave spectroscopy of the PBr radical in the X  $\Sigma$  – 3 state

J. Chem. Phys. (September 2008)

Small Low Mass Advanced PBR's for Propulsion

AIP Conference Proceedings (July 1994)





Downloaded from http://pubs.aip.org/aip/jap/article-pdf/doi/10.1063/5.0141059/16774850/093301\_1\_online.pdf

Cite as: J. Appl. Phys. 133, 093301 (2023); doi: 10.1063/5.0141059 Submitted: 2 January 2023 · Accepted: 12 February 2023 · Published Online: 2 March 2023







R. Z. Walkera) D and J. E. Foster

# **AFFILIATIONS**

Department of Nuclear Engineering and Radiological Sciences, University of Michigan, Ann Arbor, Michigan 48109, USA

a)Author to whom correspondence should be addressed: rzpinsky@umich.edu

#### **ABSTRACT**

Plasma-based water purification involves the transport of reactive species across the gas-liquid interface. This process is limited by slow diffusion driven mass transport of reactive species across the interface. Additionally, the plasma gas-liquid contact area is typically limited, contributing to reduced dose delivery. These key factors make it difficult to scale up the treatment process to input flows of industrial interest. In this work, turbulence is explored as a means to introduce a fine grain structure, thus greatly increasing the interfacial surface area, leading to large property gradients and more efficient mass transport. Such a fine scale structure can also enhance the local electric field. The test apparatus explored in this work is the packed bed reactor that places thin water jets into contact with plasma. It is theorized that fintroducing turbulence, via increasing Reynolds number in such thin jets, may enhance the effective plasma dose at fixed plasma power. In this work, changes in the flow regime, from laminar to turbulent, of water jets in a packed bed water reactor (PBR) configuration are investigated experimentally. Methylene blue dye, a model contaminant, was tested in the PBR to demonstrate enhanced treatment via reduced treatment times. Plasma surface morphology around the jets noticeably changed with the flow regime, and turbulent flow demonstrated a faster hydrogen peroxide uptake, along with slower temperature, electrical conductivity, and a pH change in a batch treatment process, compared to laminar flow. The dye was destroyed significantly faster in the turbulent flow, indicating an increased effective plasma dose.

Published under an exclusive license by AIP Publishing. https://doi.org/10.1063/5.0141059

I. INTRODUCTION

gaps in understanding, the experimentally observed induced advanced oxidation and reduction has fueled numerous investigative advanced oxidation and reduction has fueled numerous investigative advanced oxidation and reduction has fueled numerous investigative. The test apparatus explored in this work is the packed bed reactor that places thin water jets into contact with plasma. It is theorized that

The interaction of nonthermal, atmospheric pressure plasma with liquid water generates a host of reactive oxygen and nitrogen species, such as the hydroxyl radical as well as reductive species, such as solvated electrons. These species—along with UV light and the ultrasound that is produced—drive advanced oxidation, advanced reduction, and physical decomposition of organic contaminants in a solution, leading ultimately to mineralization.<sup>1,2</sup> Of particular interest is the interaction of the plasma with the liquid interface. It is here where reactive species are generated, and it is this boundary that serves as the conduit for mass transport of reactive species between the gas and liquid phase. The prevailing plasma-driven processes at the interface, both physical and chemical in origin, are not well understood. In particular, the actual dose of useful reactivity induced into the water that facilitates some change within the bulk remains ill-defined. However, in spite of advanced oxidation and reduction has fueled numerous investigations probing the efficacy of the application of nonthermal plasmas in water treatment for the removal of recalcitrant contaminants particularly those difficult to remove conventionally.<sup>2-6</sup> Indeed, efficacy at the decomposition of a range of organic contaminants in treatment volumes in the range of liters has been demonstrated. Scaling these processes up to address larger, practical values for water treatment needs process rates of  $\sim$ 150 liters/min on the lower end of the spectrum, typical of water produced by a well, and millions of liters per day on the larger end of the spectrum, common to municipality needs.

The chief limitation to scale up, whether the processing is batch<sup>4,7,8</sup> or once-through, is dose delivery. A meaningful dose must be delivered to water per unit time by the plasma to produce a reactive species concentration in solution commensurate with the level needed to achieve decomposition of the treatment volume or

process water flow rate in a reasonable amount of time, typically dictated by process water production rates. Plasma treatment is inherently a surface process as discussed earlier, occurring at the plasma-liquid interface. Owing to the reduced mean free path, plasma attachment at the interface is typically limited to micrometers, which translates into plasma attachment footprints that are sub-millimeter in diameter. Because the contact area is limited, the delivered dose is also restricted. Compounding the problem is the fact that reactive species transport is delivered diffusely into the bulk, an inherently slow process—an issue that becomes problematic with increased treatment volume.

In once-through (single pass) systems, a key to plasma-based treatment scale up is the delivery of dose (i.e., amount of reactive species transferred to the water) to the interface at levels to enable the treatment of the water as it passes the plasma applicator. Methods to improve dose delivery include the use of a multitude of plasma applicators in contact with water disposed to thin layers or the use of thin streams of water brought in contact with the plasma.<sup>3,4,7</sup> In both cases, the liquid contact surface area to volume ratio is maximized to increase dose and with thin layers, it greatly increases diffusive transport. The importance of the contact area has been described previously. As these approaches feature thin layers of water, however, they are inherently throughput-limited. Methods that increase the plasma contact area at the interface naturally present conditions for increased uptake. Additionally, since reactive species are produced in the volume between electrodes and the interface along the track of the streamer, the uptake of these species can also be enhanced if the surface area of the interface itself could be increased as well. The work described herein focuses on improving the contact area through the introduction of turbulence along the liquid surface for the purpose of increased uptake of reactive species produced by the plasma.

The reactor used in this work disposes input feed water into a number of parallel thin water jets, as can be seen in Fig. 1, in a packed bed reactor (PBR) configuration. A set of 18 straight pipe nozzles are used to produce parallel jet streams before the plasma

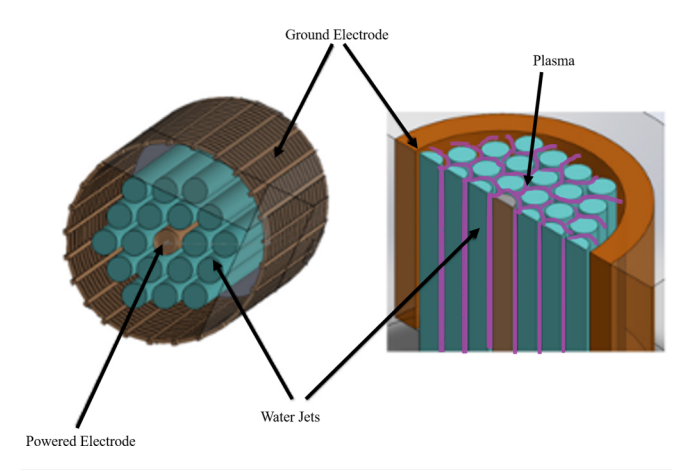


FIG. 1. Cutaway of a plasma applicator. Adapted with permission from Foster et al., J. Phys. D: Appl. Phys. 51, 293001 (2018). Copyright 2018 IOP Publishing.

head section. The high surface area to volume jets is uniformly dispersed within an annular region between a centrally located powered electrode and an outer cylindrical electrode. The electric field as calculated via an EM solver exceeds the threshold for streamer formation ( $>30\,\mathrm{kV/cm}$ ) for the applied voltages explored in this work. This arrangement promotes breakdown across all the water jets. The reactor works by generating plasma in the interstitial spaces between an array of water jets, as well as by the propagation of ionization waves along the surface of the jet streams, as inferred by visual observation of plasma formation along water jets. This is similar to that observed by Ning<sup>10</sup> and Lai<sup>11</sup> of streamers propagating along a perturbed droplet surface. This arrangement presents a larger surface area for dose absorption than that which would result from simple surface treatment of a monolithic cylinder of water typical of pipe flow. Here, the plasma generated dose is delivered primarily by surface contact and diffusion. Depending on the flow speed and showerhead geometry (which delivers the jets), the jet's flow regime can be varied from laminar to turbulent. The transition from laminar to turbulent flow in water jets is associated with instabilities that form and propagate along the surface as well 2 as spray formation as can be seen in Fig. 2 from Hoyt and Taylor.<sup>1</sup> A fine surface structure, small feature characteristic length scales, and circulation eddies are characteristic of high Reynolds number turbulent flows.

Turbulence, therefore, offers a hydrodynamic opportunity to  $\frac{i\alpha}{2}$ maximize the contact surface area, thus acting as a multiplier. In § particular, under turbulent conditions, the surface structure and, thus, the contact surface area can be greatly increased. The grain structure induced under such conditions also greatly increases gradients on all scales, which invariably enhances the diffusive transdients on all scales, which invariably enhances the diffusive transport and mixing of reactive species into the liquid.<sup>13</sup> These conditions are desirable for the treatment of contaminants in water. In the case of hydrophobic contaminants, such as per and poly-fluoroalkyl substances (PFAS) compounds, the increase in the plasma facing surface area driven by turbulence maximizes contact with the plasma, thus greatly improving decomposition efficiency. In the case of hydrophobic contaminants, such as per and poly-Associated mixing in individual jets also has the potential to bring hydrophilic short-chain compounds to the surface for treatment as well. The fine structure and the associated sharp curvature of surface water jet features can also lead to changes in the local electric field, enhancing breakdown and the propagation of ionization 8 waves. Highly turbulent structures create droplets for plasma treatment as well as incorporation of plasma generated species into the liquid via entrainment, <sup>14</sup> which provides opportunities not only for <sup>3</sup>/<sub>8</sub> air stripping and subsequent plasma treatment but also the introduction of additional vapor into the gas phase, which can improve OH radical production. The creation of what can be thought of as pores in the liquid near the surface can also occur, which also affects the local dielectric response of the liquid water as well. It is also theoretically possible for the plasma to couple to water jets electro-hydrodynamically and, thus, enhance or bring on the onset of turbulence. Though a detailed analysis of all these possible effects are beyond the scope of this work, they serve as motivating mechanisms for the investigation of the opportunities that turbulent flow may provide to enhance dose delivery to the plasma.

In this work, we investigate the effect of a flow regime (as inferred from Reynold's number) on discharge operating

FIG. 2. Water jets disposed into stagnant air taken at different distances downstream in units of a jet initial diameter (right hand side). Rich surface morphology and droplets are apparent during turbulent flow. Reproduced with permission from J. W. Hoyt and J. Taylor, J. Fluid Mech. 83(1), 119-127 (1977). Copyright 2006 Cambridge University Press.

characteristics. Here, the local Reynold's number is first varied in the absence of plasma in order to document surface morphology of jets and qualitatively infer the degree of surface area enhancement by the relative roughness of the water jet surface. To understand the effect of this roughness on plasma morphology, we next characterize the discharge response (nature of attachment) associated with the various flow regimes. We then explore the efficacy of plasma generated under turbulent water jet conditions by treating a model contaminant, methylene blue dye. The objective here is to test the hypothesis that the turbulent regime as compared to laminar or transitional flow can enhance decoloration efficiency.

What is presented here is an observed phenomenon of a discharge morphology change with a flow regime. Further

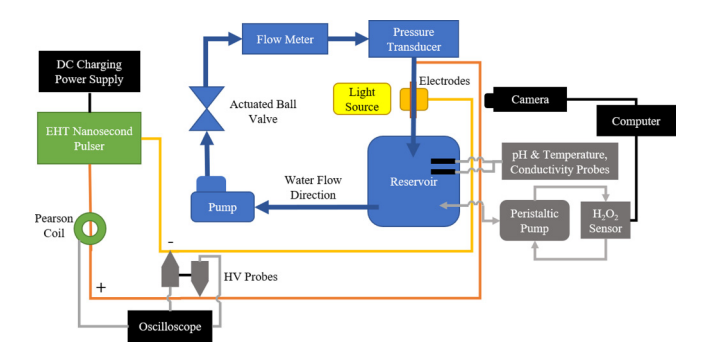


FIG. 3. Experimental setup, with blue arrows indicating the flow direction.

investigation revealed differences in treatment rates of a model dye dence that these data, while additional research is required, suggest that turbulent flow may be a factor in realizing higher decomposition rates. This is believed to be due to an increased surface area and mixing associated with turbulent flow.

#### II. EXPERIMENTAL SETUP

The experimental apparatus used in this investigation & described previously<sup>4,15,16</sup> was modified to facilitate imaging of the water jets. A cutaway of the reactor is shown in Fig. 1. As can be seen here, equally spaced water jets are generated around a centrally located stainless steel powered electrode. A stainless steel mesh surrounding the jets, with a diameter of 12.7 mm, is used as the ground electrode. The plasma is generated along the 40 mm reactor section, with room air as the carrier gas. The discharge forms in the interstitial spaces and along water jets. The water flow speed was controlled by a circulation water pump and an actuating ball valve, which allowed for the variation in the flow regimes. Water exiting the plasma head enters a reservoir that feeds the pump, facilitating recirculation. Inline sensors allow for an *in situ* flow rate (Omega FPR302), line pressure (Wika A-10), pH, temperature, conductivity (Thermo Scientific Orion STARA3290), and peroxide concentration (ATi Q46/84) measurements. In this work, the reactor operates in a recirculating batch mode configuration, shown in Fig. 3. The pulsed corona discharge was driven using an EHT nanosecond high voltage pulser. Current was measured using a fast of Pearson coil model 6600 with a usable rise time of 5 ns, and the applied voltage was monitored using two Tektronix 6515A 1000X high voltage probes. A 200 MHz Tektronix MDO3024 oscilloscope was used to collect the current voltage data.

# A. Imaging of flow and initial plasma assessment

In order to image the surface structure of the water jets, the water jets were backlit with a broadband light source and imaged with a fast-framing camera (Redlake MotionPro HS-4). As shown in greater detail in Fig. 4, which depicts a cross section of the applicator head, diffuse light was allowed to pass through the series of flowing water jets and is imaged at 5000 frames/s. The evolution of water jet

4.5 LPM, I (A) 4.5 LPM, V (kV) 11.4 LPM, I (A)

11.4 LPM, V (kV)

3

0

20

-1

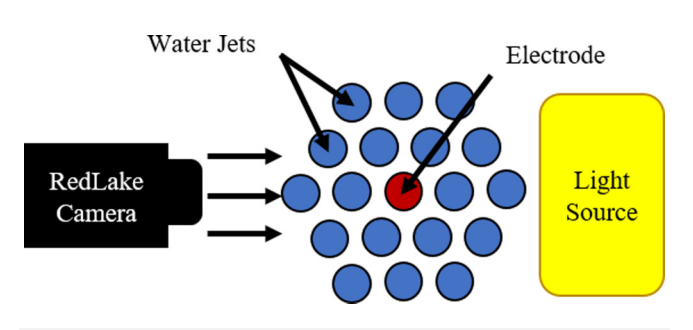


FIG. 4. Imaging scheme for assessing jet flow regimes.

morphology was characterized as a function of flow rate. Over the flow rate range explored in this work, the water jets were observed to transition from laminar, transitional, and turbulent flow.

The flow regimes, as determined from the high speed camera imagery, were then explored in the presence of plasma to understand the discharge response. As will be discussed in Sec. III B, significant changes in discharge morphology were observed in response to flow regime changes. In order to understand the impact of a flow regime on a delivered dose, measurements were made on pH, peroxide, electrical conductivity, and bulk temperature changes. Feedwater used in this investigation was room temperature de-ionized (DI, from a Millipore Milli-Q Integral 10 water purification system), with a starting conductivity of approximately  $10\,\mu\text{S/cm}$  and a starting pH of 5. At the end of each plasma test of 20 min, the temperature did not exceed 30 °C and pH averaged 4. The plasma treatment had a significant effect on the liquid conductivity, which will be discussed in Sec. III.

The discharge power was explored in conjunction with the flow rate changes (laminar, transitional, and turbulent). Though the integrated power changed over time, due to changes in the water matrix, a constant DC charging voltage (to the nanosecond pulser) and a discharge frequency were applied. The pulse peak voltages were around 11.5 kV at both 2 and 1 kHz repetition rate and 12.0 kV at a 2 kHz repetition rate. Note that the applied peak voltages are similar in amplitude, but the waveform structure itself did vary reflecting the response of the load to the variation in the flow regime. Figure 5 illustrates typical waveforms for transition and turbulent flow regimes. As can be seen in Fig. 5, there is a substantial structure to the voltage and current waveforms that changes with the flow rate. These sample waveforms shown remained stable throughout the discharges, with the exception of a high-power mode observed in the 12 kV case, which will be discussed in Sec. III. Of particular note, the amplitude of the current peaks under turbulent conditions is smaller in amplitude in comparison with that observed during the transition flow regime. This is consistent with the more diffuse glow observed during the turbulent regime in comparison with the localized constricted attachments observed during transitional flow.

The discharge power  $(P_D)$  was estimated by direct integration of the I-V waveform, as shown in Eq. (1). In this,  $f_p$  is the discharge frequency,  $t_p$  is the pulse duration,  $V_+/V_-$  are the voltages on the high and low voltage sides of the floating power supply, and

FIG. 5. Sample current (I) and voltage (V) waveforms produced by a nanosecond pulser. The conditions shown are run with a 2 kHz discharge frequency for the transitional and turbulent flow rate cases (4.5 and 11.4 LPM) to illustrate the changes in the I-V structure for different flow regimes.

Time (s)

 $I_t$  is the discharge current. It is to be noted that the waveform can consist of contributions from displacement, ohmic dissipation, and reflected power. Owing to the overall complexity of the waveform, no attempt in this work was made to correct for these dynamic effects. Rather, this complexity is simply noted, and detailed waveform analysis is beyond the scope of this work. In this context, the form analysis is beyond the scope of this work. In this context, the integrated power is used as an indicator of trends in absorbed power. Through these experiments, power is estimated at various time intervals based on sample I–V curves,  $P_D = f_p \int_0^{t_p} (V_+(t) - V_-(t)) I_t(t) \, dt. \tag{1}$  B. Plasma dose delivery—The batch process
In the work presented here, the reactor was operated in a batch mode, treating a fixed volume of water. One might expect that the dose delivery depends on the flow rate; however, it can be

$$P_D = f_p \int_0^{t_p} (V_+(t) - V_-(t)) I_t(t) dt.$$
 (1)

that the dose delivery depends on the flow rate; however, it can be shown that the dose delivery per unit time is actually independent of the flow rate in a recirculating system. This is true as long as the plasma pulse period is much smaller than the residence time of a fluid element in the plasma section (so that the fluid element effectively experiences "constant" plasma as it passes through). The residence time,  $\tau$ , of a fluid element in the plasma section is inversely proportional to the fluid velocity v,

$$\tau = \frac{L}{\nu},\tag{2}$$

where L is the length of the plasma section (40 mm).

The cycling frequency,  $f_{cycle}$ , of a fluid element of water going through the plasma section with area A is related to the volumetric flow rate  $Q = \nu A$  and the batch volume, V,

$$f_{cycle} = \frac{Q}{V} = \frac{vA}{V}.$$
 (3)

Therefore, with fixed geometry and constant volume, the cycling of a fluid element will be proportional to v. The dose rate, therefore, will be a product of this cycling frequency and the residence time of the water in the plasma section, multiplied by some proportionality constant, that is the plasma dose delivery rate s (the rate at which the plasma contacts the liquid),

Dose Rate = 
$$sf_{cycle}\tau = s\frac{vA}{V}\frac{L}{v} = const.$$
 (4)

This dose rate is, therefore, independent of the flow velocity. This insensitivity to the flow rate allows for a comparison of fluid regimes. In this work, the pulse frequencies that were explored were in the 1-2 kHz range with liquid flow rates in the 1-10 LPM range resulting in fluid element residence times of approximately 100 times the plasma pulse period, which satisfies the conditions where dose is flow rate independent.

### C. Methylene blue tests

In order to better understand flow rate induced changes to delivered dose to the water, the plasma is used to decolor water spiked with a model contaminant dye, methylene blue (MB, C<sub>16</sub>H<sub>18</sub>N<sub>3</sub>SCl). The MB salt dye is representative of those used in the textile industry.<sup>17</sup> Such dyes in wastewater are persistent in the environment owing to their recalcitrant nature and can lead to ecosystem damage. The complete oxidation of MB produces CO2, HNO<sub>3</sub>, H<sub>2</sub>SO<sub>4</sub>, and HCl. For this experiment, the plasma was generated at a fixed pulse frequency of 2 kHz with a peak voltage of 11.5 kV. For the three tested flow regimes (laminar, transitional, and turbulent), an initial MB concentration of approximately 40 ppm (0.125 mM) in DI water was treated for a total of 120 min. The concentration of MB in the simulated wastewater was assessed every 15 min for a total of 2 h, requiring 8 ml extractions from the 11 reservoir for each measurement. Less than 7% of the total volume is lost as a result of these periodic extractions. The variation in MB concentration over time was accessed by measuring the solution's absorbance around 609 nm in a spectrophotometer (Thermo Fisher Genesys) and using Beer's law, 20,21 where a calibration curve had been established between approximately 0.4 and 40 ppm.

#### III. RESULTS AND DISCUSSION

# A. Feedwater jet morphology variations with the flow speed

Understanding the effect of a flow regime on an adsorbed plasma dose is a key objective of this work. The flow regime is primarily characterized by the Reynolds number. The Reynolds number, Re, relates inertial forces experienced by the flow to viscous forces, which tend to impede the flow,

$$Re = \frac{\rho v d}{\mu},\tag{5}$$

where the variable  $\rho$  is the density of the liquid, v is the characteristic velocity, d is the characteristic diameter, and  $\mu$  is the dynamic viscosity. This equation can be recast in terms of a flow rate, which is convenient in this work where the only free variable is essentially a flow rate as the shower head nozzle diameter is fixed. In this case,

$$Re = \frac{4\rho F}{\pi \mu d_i N_i},\tag{6}$$

where  $N_i$  is the number of nozzles,  $d_i$  is an individual jet diameter, and F is the total flow rate. In general, pipe flow characterized with an Re < 2300 is typically laminar, while flows with Re between 2300 and 4000 are considered transitional. For flows with Re greater than 4000, the flow is considered turbulent. <sup>22</sup>

Another parameter useful in characterizing the flow is the Weber number, We. This parameter yields the relative importance of inertial forces to surface tension forces and is often used in the analysis of multiphase flows. The Weber number is defined as

$$We = \frac{\rho v^2 d_j}{\sigma},\tag{7}$$

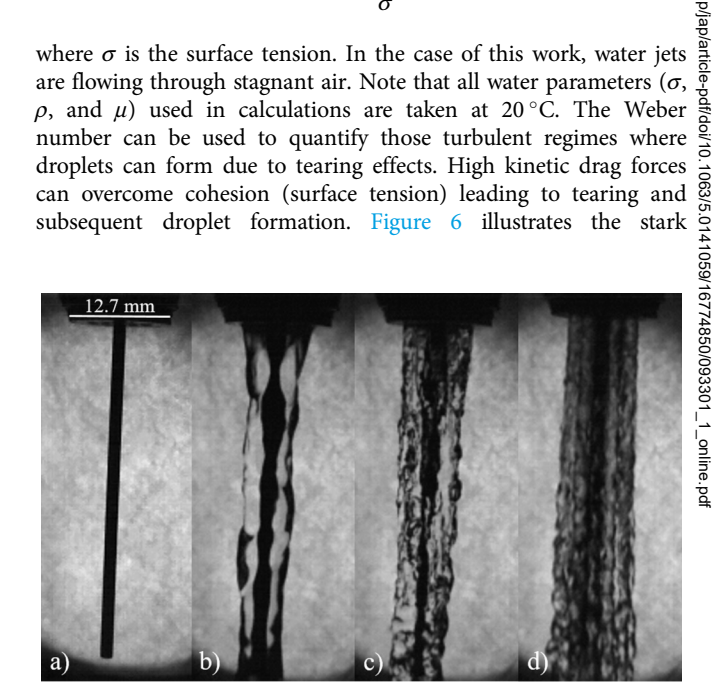


FIG. 6. Imaged flow regimes of a packed bed reactor: (a) Plasma applicator without water flow (powered electrode shown); (b) laminar flow case—flow rate 1.1 LPM, Re = 840, and We = 6.2; (c) transitional flow case—flow rate 4.5 LPM, Re = 3358, and We = 99; and (d) turbulent flow case—flow rate 11.4 LPM, Re= 8395, and We = 620.

differences in flow morphology as a function of flow rate for the apparatus used in this work.

In addition, it has been shown in the literature that the scalar properties of turbulent flow depend highly on the inlet conditions of the jet.<sup>23–25</sup> This reactor may be approximated as a long pipe nozzle, which produces a fully developed turbulent pipe velocity flow profile<sup>23</sup> since the nozzle length/diameter (L/D) = 24\*D is long enough to become fully developed.2

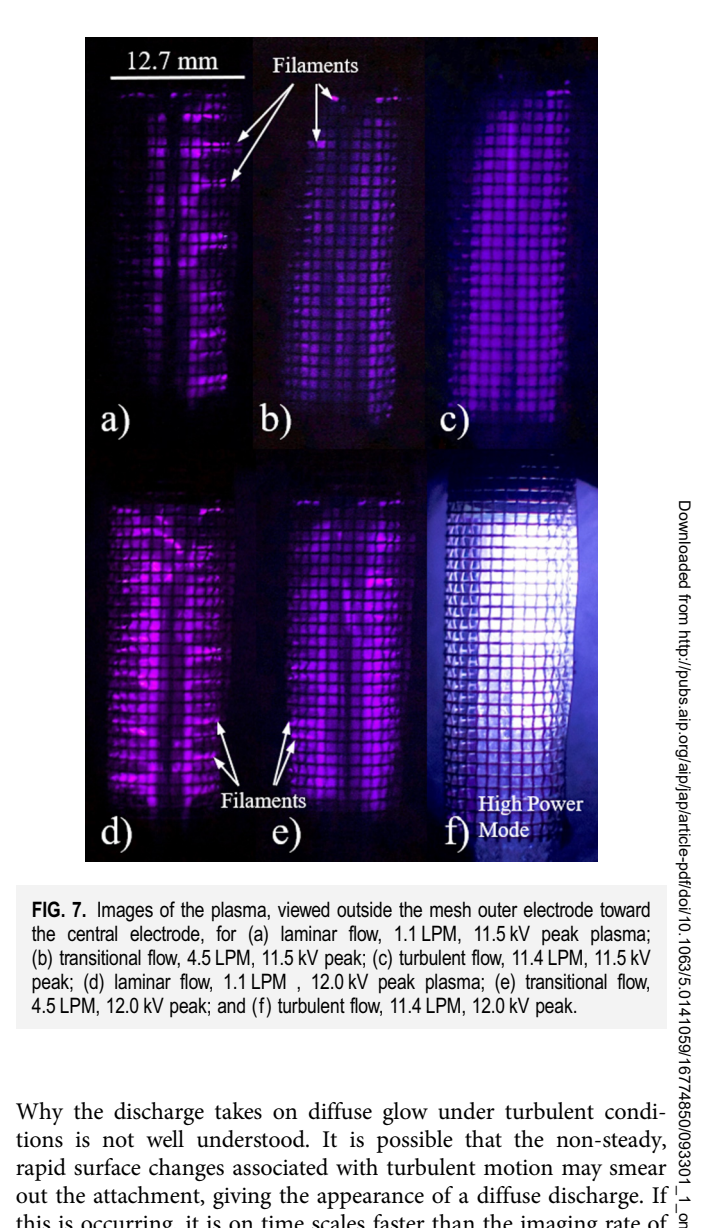
The flow conditions tested in this reactor consist of a laminar, transitional, and turbulent flow case, corresponding to 1.1, 4.5, and 11.4 LPM (0.3, 1.2, and 3.0 GPM). These correspond to Reynolds numbers of 840, 3358, and 8394, respectively. The range of flow regimes are directly accessible with the reactor as can be seen in Fig. 6.

The surface morphology of the water jet transitions from smooth in the laminar regime with only long wavelength surface perturbations to the highly structured surface associated with the turbulent flow. The length scale of the surface perturbations under this regime is considerably smaller than that observed in the laminar case. As can be seen in Fig. 6, the overall external boundary of the water jet ensemble also varies with the flow regime as one might expect, with that of the turbulent regime appearing wider, due to the separation of individual jet streams in the shower head at the higher flow rates. In this regard, not even considering the fine scale structure, the projected physical area (outer surface area) in the turbulent flow regime is larger.

The showerhead geometry at lower flow rates impacts overall morphology of the ensemble of water jets. Under such conditions, the jets are susceptible to instabilities. For example, for a set of close-packed water jets, a region of low pressure develops in between the jets. This low pressure region causes individual jets to eventually merge together at some distance from the entrance. The merging of jets at low flows in this work appears to be consistent with this effect, which is clearly visible as can be seen in Fig. 6(b), where there are no distinguishable jets in the laminar case. The Coanda effect could also contribute to merging of jets, as the central electrode provides a surface for the jets to adhere.

#### B. Plasma flow regime coupling

It was observed that the appearance of the plasma attachment at the water jet surface was highly sensitive to the water jet flow regime. The variation in the plasma structure and brightness with changes in the flow rate can be seen in Fig. 7, as viewed outside the outer mesh electrode, with the central electrode at the center. The laminar flow regime tended to favor filament-like discharge attachments. With increasing flow rate, the plasma attachment was observed to become more diffuse. Interestingly, the transition flow regime manifested discharge morphology that included localized attachments upon a backdrop of diffuse plasma glow. In the turbulent regime, the discharge takes on fully the appearance of uniform glow. In general, pulsed corona attachment to smooth surfaces is typically filamentary. It is apparent that surface perturbations along the water jet surface alter overall discharge topology. As Re increases, the degree of water jet surface perturbation increases. At fully turbulent, these surface structures are microscopic and are, thus, of the order of the length scale of the filament footprint itself.



out the attachment, giving the appearance of a diffuse discharge. If \( \( \) this is occurring, it is on time scales faster than the imaging rate of the camera, 13 frames/s in this case. Memory effects associated with surface charging, which favors filamentary discharges, may be disrupted owing to the rapid recycling of the water jet surface that occurs in the turbulent regime. In this regard, the non-steady water surface in the turbulent regime may not favor localized attachments. In any case, the brighter diffuse glow at the higher power case, in particular, suggests greater plasma attachment and coverage of the water jets, which should manifest an inherently larger plasma-liquid surface contact area. An increased contact area should translate into better dose delivery. Greater dose delivery should, therefore, be reflected in the rate at which the particular plasma mode can remove contaminants from the water. This reasoning motivated the MB tests to assess the dependence of dose delivery upon the flow regime.

# C. Assessing delivered dose

Changes in water quality and energy delivered due to plasma exposure were characterized by monitoring changes in pH, water temperature, electrical conductivity, and peroxide concentration vs treatment time. pH changes are related to the production of NO<sub>x</sub> species in the gas phase. Electrical conductivity is associated with the diffusion of ions in the gas phase that diffuse into solution. Peroxide is also produced in the gas phase as well at the plasmaliquid interface. These parameters are a function of the gas phase radical production rate and the physical contact area presented by the liquid water jet. These changes are depicted in Fig. 8 where the difference between the sampled and starting condition is plotted as a function of treatment time. Uncertainty for measured quantities is not depicted in the figure for clarity, although they are small. Note that the starting pH and conductivity were the same in all cases. At the same applied voltage amplitude and pulse frequency, there is a clear difference in parameters as a function of flow rate. The H<sub>2</sub>O<sub>2</sub> and electrical conductivity increased in all cases approximately linearly. The pH and water temperature, on the other hand, varied exponentially, with the pH dropping over time and the water temperature increasing with time. The temperature changes are due to power deposited into the water by the plasma balanced by evaporation at the interface.<sup>5</sup> As it is a batch system, the power is deposited into a fixed volume, and thus, a slow exponential increase can be expected since the water temperature will be proportional to the difference between itself and the plasma gas.

For the operating conditions of 11.5 kV at 1 and 2 kHz, the magnitude of the pH changes was the largest for the laminar flow regime, while the turbulent flow regime manifested the slowest rate of change. Likewise, the liquid temperature change was also the lowest in the turbulent regime. This cooler operating temperature may also be due to a combination of more efficient convective cooling associated with higher flow speed through the air and the increased observed surface area of the water jet in the turbulent regime. The peroxide concentration increased at a greater rate in the turbulent flow regime. This observation suggests more efficient mass transfer of plasma species in the turbulent regime as well. It may also mean greater efficiency in peroxide production, suggesting a gas phase plasma chemistry effect. Surprisingly, the magnitude of the conductivity changes of the water treated in the turbulent 8 regime was the smallest. This is indeed consistent with the comparatively smaller changes in the pH as compared with water treated in the laminar and transitional regime. The reduced overall change in pH implies that the overall uptake rate of  $NO_x$  species is for some reason reduced. Because pH reduction is largely dependent on  $NO_x$  species formation, filamentary discharges with higher gas

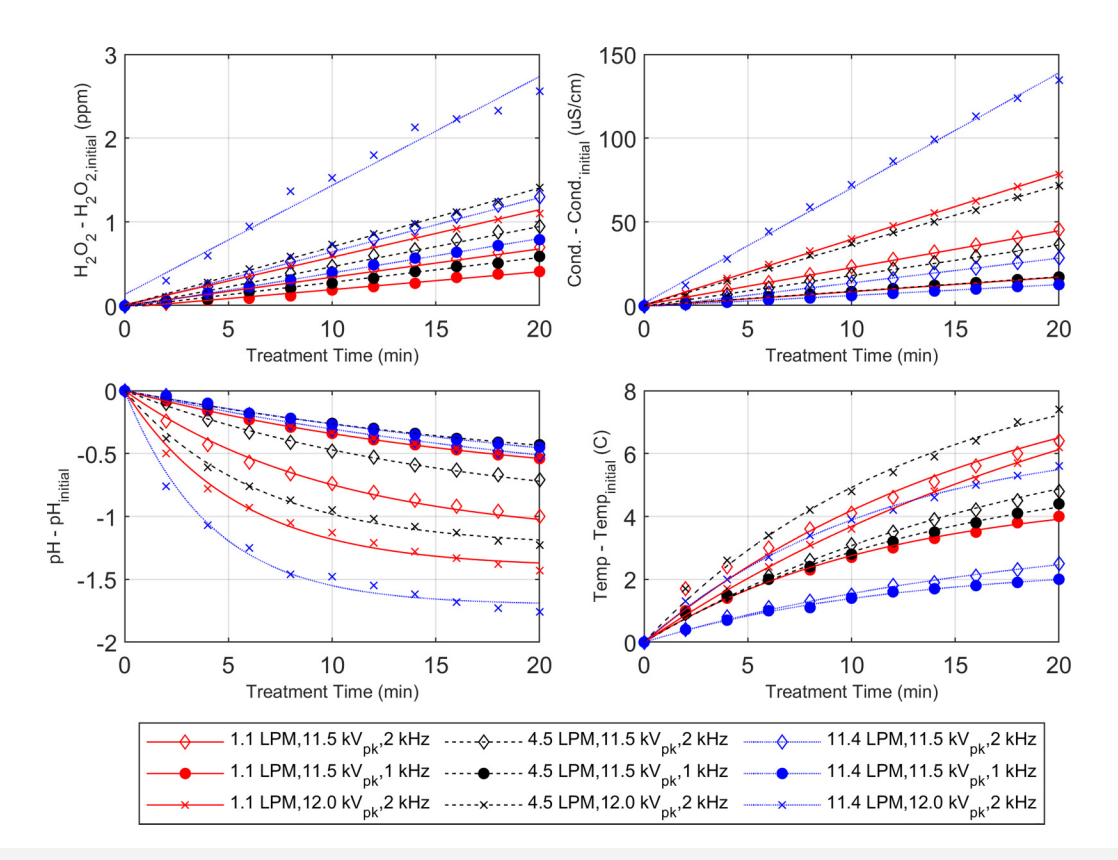


FIG. 8. Changes in peroxide (H<sub>2</sub>O<sub>2</sub>) concentration (top left), electrical conductivity (top right), pH (bottom left), and bulk water temperature (bottom right) for an 11.5 kV, a 2 kHz discharge, an 11.5 kV, 1 kHz discharge, and a 12.0 kV, 2 kHz discharge at 1.1(laminar), 4.5 (transitional), and 11.4 LPM (turbulent) flow rates.

temperatures may be more efficient in producing gas phase  $NO_x$  that actually reaches the water surface. It should also be noted under certain conditions that  $NO_x$  in solution suppresses peroxide formation.<sup>27</sup>

It should be noted that the differences in solution changes observed in the laminar and turbulent cases were not unexpected, given the merging that occurs in the laminar case, making it appear as a single water jet flowing along the inner electrode. This changes the nature of the discharge, as well as provides a much smaller contact area for dose delivery. However, the transitional and turbulent flow cases do have separated jets, but also interestingly show a difference in dose delivery, providing evidence that this phenomenon is not purely geometry based, but rather a flow regime plays a role.

Similar patterns are observed in both the 1 and 2 kHz discharges at 11.5 kV. However, rates of change are not halved with halving the frequency, indicating a nonlinear effect. Trends in the production rate of  $\rm H_2O_2$  saw a similar 37%–38% decrease in all flow regimes by decreasing the frequency from 2 to 1 kHz, starting at  $3.4*10^{-2}$  ppm/min for laminar flow,  $4.8*10^{-2}$  ppm/min for transitional flow, and  $6.5*10^{-2}$  ppm/min for turbulent flow. As the data suggest, decreasing the pulse frequency decreases the rate of dose delivered. The pulse rate changes the rate at which peroxide is produced both in the gas phase and at the interface, promoting this nonlinear effect on peroxide production.

Interestingly, in the higher peak voltage case of 12.0 kV, a significant increase in peroxide production and rate of concentration rise was observed. It should be pointed out that at this higher voltage mode, the discharge was not strictly diffuse but rather included the random occurrence of an intense, bright streamer. This mixed mode is shown in Fig. 7. This mode is particularly apparent at low liquid conductivity and tends to become less frequent as conductivity increases with time. 16 It is difficult to assess the mixed mode's power contribution as it occurs randomly and typically early on while liquid conductivity is low. It is postulated that its occurrence is due to the higher gap electric field because at reduced electrical conductivity of the liquid water, the interface acts more of a dielectric rather than a leaky capacitor. It apparently has a clear impact on the delivered dose, as this high-power case is observed to have the largest peroxide production and conductivity change, along with the largest pH drop. The temperature also increased more in this case than in either of the other turbulent cases, although not the largest temperature increase over all cases.

A full discussion of the reaction kinetics driven by this particular reactor leading to the observed changes in the liquid water is beyond the scope of this work; however, related reaction chemistry leading to such changes may be found elsewhere. The primary species of interest for this work include long-lived species in plasma discharge, including  $H_2O_2$ ,  $O_3$ , and secondary species, formed in the liquid, such as  $NO_x$  ( $NO_2^-$  and  $NO_3^-$ ). Other species important for plasma advanced oxidation and reduction processes include the hydroxyl radical  $O_2^+$ , solvated electrons  $e_{aq}$ , atomic oxygen  $O_3$ , singlet oxygen  $O_3^+$ , and the superoxide radical  $O_2^-$ , as well as UV radiation. See that in air plasma discharges, especially at low pH, nitrite and peroxide react to produce peroxynitrite, lowering  $O_3^+$ , a key oxidant, concentration. However, reaction rates are relatively slow and are

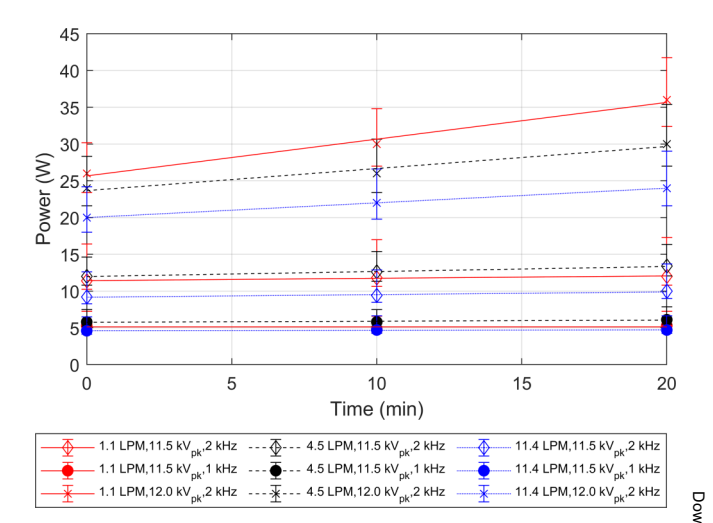


**FIG. 9.** Plasma power as a function of time for 11.5 kV, 2 kHz discharge; an 11.5 kV, 1 kHz discharge; and a 12.0 kV, 2 kHz discharge at 1.1 (laminar), 4.5 (transitional), and 11.4 LPM (turbulent) flow rates.

not expected to have a large impact on measured  $H_2O_2$  concentrations due to *in situ*, real time sensors. These interferences must be understood for advanced oxidation process (AOP) optimization in water treatment systems.

It was observed that for all cases, the deposited power tended to increase with time, albeit at different rates, as depicted in Fig. 9. The increases in power deposition were also observed in the methylene blue decoloration experiments, which had a much longer test duration (120 min). The increase in the power deposition is most likely due to the associated observed increase in electrical conductivity. Here, the solution acts more resistive rather than as a dielectric; therefore, in volume, dissipation contributes to power loss. It should be noted, however, that the calculated deposited power was not equal for each flow rate case, with the lowest starting power occurring in the turbulent flow case and the highest starting deposited power occurring for laminar flow. This may be explained by the very nature of the attachments in the various flow regimes. Interestingly, at the lowest pulse frequency investigated (1 kHz), the deposited power was similar for all cases.

## D. Destruction of methylene blue

The next step was to assess the impact of the observed discharge flow modes on the decomposition of a model containant. Note that this experiment was not meant to achieve the highest treatment degradation rates as found in the literature, <sup>30</sup> but rather to observe comparative changes induced by different flow regimes. A 0.125 mM (40 ppm) solution of MB was plasma treated in the reactor operating in the three flow regimes, in the 11.5 kV operating condition. This power was selected to ensure that the discharge did not enter the high-power mixed mode, as described previously. The MB degradation as a function of time is shown in Fig. 10. A greater than 2-log reduction in MB from around 40 ppm to less than

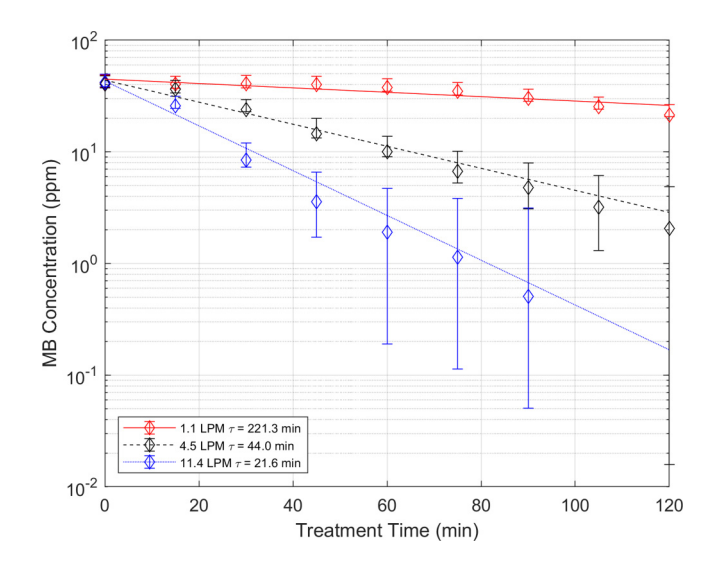


**FIG. 10.** Methylene blue (MB) destruction for laminar, transitional, and turbulent flow cases with the same plasma treatment conditions. Note that there are no data points for the 11.4 LPM turbulent case at 105 and 120 min since the treated water falls below the detection limit of the spectrophotometer.

0.5 ppm is observed in the turbulent flow regime over 90 min of treatment. Note that the final two data points of the turbulent case are not plotted since they were at the lower limit of detection for the spectrophotometer. The time constant for destruction (from the first order exponential decay characteristics) varied substantially at the different flow rates, from around 22 min for the turbulent case to 221 min in the laminar case, with the transitional case falling in between with a time constant of destruction of 44 min. This result indicates that, holding other conditions the same, including voltage, treatment volume, and time, the plasma attachment associated with the turbulent mode greatly improves removal efficiency. In addition to the plasma morphology and attachment to the liquid, there are also mass transfer effects at the gas-liquid interface. In laminar flow, mass transfer is dominated by molecular transport, governed by Fick's law of diffusion. However, when the flow becomes turbulent, transport processes become dominated by momentum diffusion via turbulent eddy motion, where molecular diffusion processes play a much less significant role. In the turbulent regime, as the flow rate increases, the length scales of the smallest eddies decrease, promoting even faster transport of species into the bulk liquid. These confounding effects both contribute to reactive species uptake and decoloration of MB.

During MB treatment, the deposited power did not remain constant during treatment. The laminar and transitional cases exhibited substantial (more than double) power increases over the treatment time, from 13 W initially, increasing at 0.16 W/min, and 0.14 W/min to 30 and 28 W, respectively, at 105 min of treatment, while the turbulent case exhibited a significantly slower rate of increase. For the turbulent case, the starting deposited power was 10 W, increasing at around 0.04 W/min to 14 W at 105 min of treatment. The smaller increase in deposited power in the turbulent

case is likely related to changes in electrical conductivity of the solution. As discussed in the de-ionized water tests, operation in the turbulent regime realized the smallest change in conductivity, which translates into reduced dissipation in the solution. Again, while left to future work, this does suggest cooler plasma temperatures in the turbulent case, leading to reduced production of  $NO_x$  ions, for example, which can otherwise drive up the electrical conductivity.

The MB decoloration rate as a function of input energy can be estimated using the electrical efficiency per order  $(E_{EO})$ , a figure of merit used to compare relative energy efficiencies for different AOP processes.<sup>31</sup> It describes the energy requirements for a 1-log reduction of contaminant removal exhibiting first order kinetics. In this work,  $E_{EO} = \frac{P}{(V/t)\log_{10}(c_i/c_i)}$ , where P is the electrical power, V is the treatment volume, t is the treatment time, and  $c_i$  and  $c_f$  are initial and final concentrations, respectively, for a batch process. In this work,  $E_{EO}$  varies as a function of treatment time due to the increasing electrical power requirements as a function of treatment time (due to increasing electrical conductivity of the water). The average  $E_{EO}$  for 1-log removal of MB can be calculated from the average power requirement and treatment time in the plasma reactor. The average  $E_{EO}$  for laminar flow (1.1 LPM), extrapolated assuming a linear power increase, is 206 kWh/m<sup>3</sup> of treatment. For 4.5 LPM,  $E_{EO}$  is approximately 31 kWh/m<sup>3</sup>. For turbulent flow (11.4 LPM), average  $E_{EO}$  is  $7 \, \text{kWh/m}^3$ . The transitional and turbulent  $E_{EO}$ values were comparable to other plasma treatments as reported by Miklos et al.<sup>3</sup>

## IV. CONCLUSION

The influence of interfacial turbulence at a gas-liquid interface in the presence of plasma was studied using pulsed corona discharge in the presence of water jets generated by a showerhead applicator. It was found that discharge morphology and dose delivered to the water were highly dependent on the flow regime. Indeed, for the laminar flow case, the discharge consisted of localized filament attachments. The discharge attachment in the case of the turbulent regime was found to be diffuse with a significant coverage/plasma-liquid contact area.

erage/plasma-liquid contact area.

Changes in the solution chemistry as inferred by pH and liquid conductivity were highly sensitive to the flow regime. The turbulent flow regime exhibited more hydrogen peroxide production, with a less change in conductivity, pH, and temperature, as well as discharge power. This was seen for the most part even when the discharge frequency was halved or the applied voltage was increased. The observation of lower power deposition in the turbulent regime was consistent with the measured reduced solution conductivity relative to the other flow regimes despite a similar input voltage. Further investigation of this effect is warranted, including statistical analysis of the significance of differences observed in these initial experiments. When a model organic contaminant, methylene blue, was added to the water, the efficacy of turbulent discharge was realized, with a significantly faster destruction rate compared to the laminar and transitional discharges. The data suggest the flow regime or, more broadly, the stability of the interface may play an important role in mass transport and, thus, reactive species uptake. In this work, the non-steady interface

associated with the turbulent mode was shown to be the most effective one at species uptake and decomposition of the model contaminant MB. It is theorized that the enhanced surface area and mixing associated with the turbulent regime not only favors a more uniform discharge, it also improves contact with the plasma produced. Though left for further research, the gas phase chemistry of the diffuse mode may be quite different from the filamentary modes owing to a reduced temperature, which may facilitate the production of favorable compounds, such as hydrogen peroxide, at the expense of reduced production of  $NO_r$  species.

The observed changes in plasma attachment morphology and associated delivered dose with variations in the flow regime suggest opportunities for the optimization of plasma water reactor efficiency, regardless of its geometry. The introduction of turbulence to the liquid interface provides yet another avenue to tailor the magnitude of the delivered dose. Additionally, owing to the enhanced mixing associated with turbulent flows, introduction of turbulence may also offer a means to treat larger volumes per unit time, thus paving the way for another approach to scale up, including paving the way for the realization of once-through continuous flow through systems.

E/N was not measured locally in this work but likely it is enhanced at the surface in the turbulent regime. A key question naturally arises: which effect is more important: enhanced surface area/mixing or locally enhanced E/N due to small length scale perturbations at the surface. Either process has the potential to greatly enhance the delivered dose. Future investigations should consider how to separate these two processes to determine which is the dominant transport mechanism.

#### **ACKNOWLEDGMENTS**

This work was supported by the NSF PEAB (Grant No. 1747739), the NSF GRFP, the RACER Trust, and the Anthropocene Institute.

# **AUTHOR DECLARATIONS**

#### Conflict of Interest

The authors have no conflicts to disclose.

#### **Author Contributions**

R. Walker: Data curation (equal); Formal analysis (equal); Writing original draft (equal); Writing - review & editing (equal). J. Foster: Conceptualization (equal); Funding acquisition (equal); Project administration (equal); Supervision (equal); Writing - original draft (equal); Writing - review & editing (equal).

### DATA AVAILABILITY

The data that support the findings of this study are available within the article.

#### REFERENCES

<sup>1</sup>A. A. Joshi, B. R. Locke, P. Arce, and W. C. Finney, "Formation of hydroxyl radicals, hydrogen peroxide and aqueous electrons by pulsed streamer corona discharge in aqueous solution," J. Hazard. Mater. 41, 3-30 (1995).

- <sup>2</sup>B. Locke, M. Sato, P. Sunka, M. Hoffmann, and J.-S. Chang, "Electrohydraulic discharge and nonthermal plasma for water treatment," Ind. Eng. Chem. Res. 45, 882-905 (2006).
- <sup>3</sup>M. A. Malik, A. Ghaffar, and S. A. Malik, "Water purification by electrical discharges," Plasma Sources Sci. Technol. 10, 82 (2001).
- <sup>4</sup>J. E. Foster, S. Mujovic, J. Groele, and I. M. Blankson, "Towards high throughput plasma based water purifiers: Design considerations and the pathway towards practical application," J. Phys. D: Appl. Phys. 51, 293001 (2018).
- <sup>5</sup>P. Bruggeman, M. J. Kushner, B. R. Locke, J. G. Gardeniers, W. Graham, D. B. Graves, R. Hofman-Caris, D. Maric, J. P. Reid, E. Ceriani et al., "Plasmaliquid interactions: A review and roadmap," Plasma Sources Sci. Technol. 25, 053002 (2016).
- <sup>6</sup>J. E. Foster, "Plasma-based water purification: Challenges and prospects for the future," Phys. Plasmas 24, 055501 (2017).
- <sup>7</sup>P. Ajo, S. Preis, T. Vornamo, M. Mänttäri, M. Kallioinen, and M. Louhi-Kultanen, "Hospital wastewater treatment with pilot-scale pulsed corona discharge for removal of pharmaceutical residues," J. Environ. Chem.
- Eng. 6, 1569–1577 (2018).

  <sup>8</sup>R. K. Singh, N. Multari, C. Nau-Hix, R. H. Anderson, S. D. Richardson, S. D. Richardson, G. W. Thorard, "Rapid removal of poly-and perfluorinated compounds from investigation-derived waste (IDW) in a pilot-scale plasma reactor," Environ. Sci. Technol. 53, 11375-11382 (2019).
- G. R. Stratton, C. L. Bellona, F. Dai, T. M. Holsen, and S. M. Thagard, "Plasma-based water treatment: Conception and application of a new general
- principle for reactor design," Chem. Eng. J. 273, 543–550 (2015).

  10 W. Ning, J. Lai, J. Kruszelnicki, J. E. Foster, D. Dai, and M. J. Kushner, "Propagation of positive discharges in an air bubble having an embedded water droplet," Plasma Sources Sci. Technol. 30, 015005 (2021).
- 11 J. Lai and J. E. Foster, "Experimental observation of interfacial oscillations and gas-liquid boundary." Plasma Sources Sci Technol 28, 125003 (2019) gas-liquid boundary," Plasma Sources Sci. Technol. 28, 125003 (2019).

  12 J. W. Hoyt and J. Taylor, "Waves on water jets," J. Fluid Mech. 83(1), 119–127
- 13J. C. Lamont and D. Scott, "An eddy cell model of mass transfer into the surface of a turbulent liquid," AIChE J. 16, 513-519 (1970).
- 14H. Chanson, "Turbulent air-water flows in hydraulic structures: Dynamic sim-
- 14H. Chanson, "Turbulent air–water flows in hydraulic structures: Dynamic similarity and scale effects," Environ. Fluid Mech. 9, 125–142 (2009).

  15J. E. Foster and S. Mujovic, "Plasma water purifier having packed bed discharges with water dielectric barriers," U.S. patent 10,662,086 (26 May 2020).

  16S. Mujovic, "The plasma water reactor: A geometric approach to scaling electric discharges for water treatment," Ph.D. thesis (University of Michigan, 2019).
- tric discharges for water treatment," Ph.D. thesis (University of Michigan, 2019).
- tric discharges for water treatment," Ph.D. thesis (University of Michigan, 2019). 17K. Dutta, S. Mukhopadhyay, S. Bhattacharjee, and B. Chaudhuri, "Chemical oxidation of methylene blue using a fenton-like reaction," J. Hazard. Mater. 84, 86 57-71 (2001).
- 18A. Mills, R. H. Davies, and D. Worsley, "Water purification by semiconductor photocatalysis," Chem. Soc. Rev. 22, 417-425 (1993).

  19K. Sopajaree, Photocatalytic Oxidation of Methylene Blue by Titanium Dioxide
- in an Integrated Photoreactor-Membrane Filtration Unit (The University of Texas at Arlington, 1997).
- 20 M. Magureanu, D. Piroi, F. Gherendi, N. B. Mandache, and V. Parvulescu, "Decomposition of methylene blue in water by corona discharges," Plasma Chem. Plasma Process. 28, 677-688 (2008).
- 21 J. E. Foster, G. Adamovsky, S. N. Gucker, and I. M. Blankson, "A comparative study of the time-resolved decomposition of methylene blue dye under the action of a nanosecond repetitively pulsed DBD plasma jet using liquid chromatography and spectrophotometry," IEEE Trans. Plasma Sci. 41, 503-512 (2013).
- W. Haberman and J. John, Introduction to Fluid Mechanics (Prentice Hall, 1988)
- 23C. Ball, H. Fellouah, and A. Pollard, "The flow field in turbulent round free jets," Prog. Aeronaut. Sci. 50, 1–26 (2012).
- <sup>4</sup>J. Mi, D. Nobes, and G. Nathan, "Influence of jet exit conditions on the passive scalar field of an axisymmetric free jet," J. Fluid Mech. 432, 91-125

<sup>26</sup>V. Patel and M. Head, "Some observations on skin friction and velocity profiles in fully developed pipe and channel flows," J. Fluid Mech. 38, 181–201 (1969).

27B. Chen, Y. Huang, Q. Zhang, D. D. Dionysiou, L. Wang, and J. Li, "Formation of nitrite and hydrogen peroxide in water during the vacuum ultraviolet irradiation process: Impacts of pH, dissolved oxygen, and nitrate concentration," Environ. Sci. Technol. 55, 1682–1689 (2021).

<sup>28</sup>R. Zhou, R. Zhou, P. Wang, Y. Xian, A. Mai-Prochnow, X. Lu, P. Cullen, K. K. Ostrikov, and K. Bazaka, "Plasma-activated water: Generation, origin of reactive species and biological applications," J. Phys. D: Appl. Phys. 53, 303001 (2020).

<sup>29</sup>P. Lukes, E. Dolezalova, I. Sisrova, and M. Clupek, "Aqueous-phase chemistry and bactericidal effects from an air discharge plasma in contact with water: Evidence for the formation of peroxynitrite through a pseudo-second-order post-discharge reaction of H<sub>2</sub>O<sub>2</sub> and HNO<sub>2</sub>," Plasma Sources Sci. Technol. 23, 015019 (2014).

<sup>30</sup>M. A. Malik, "Water purification by plasmas: Which reactors are most energy efficient?," Plasma Chem. Plasma Process. **30**, 21–31 (2010).

<sup>31</sup>J. R. Bolton, K. G. Bircher, W. Tumas, and C. A. Tolman, "Figures-of-merit for the technical development and application of advanced oxidation technologies for both electric-and solar-driven systems (IUPAC technical report)," Pure Appl. Chem. 73, 627–637 (2001).
 <sup>32</sup>D. B. Miklos, C. Remy, M. Jekel, K. G. Linden, J. E. Drewes, and U. Hübner,

<sup>32</sup>D. B. Miklos, C. Remy, M. Jekel, K. G. Linden, J. E. Drewes, and U. Hübner, "Evaluation of advanced oxidation processes for water and wastewater treatment—A critical review," Water Res. 139, 118–131 (2018).